ELSEVIER

Journal of Contaminant Hydrology 55 (2002) 113–135

JOURNAL OF Contaminant Hydrology

www.elsevier.com/locate/jconhyd

Kinetic modeling of virus transport at the field scale

Jack F. Schijven [a,b,*], Jiří Šimůnek [c,1]

[a] *National Institute of Public Health and the Environment, Microbiological Laboratory for Health Protection, P.O. Box 1, 3720 BA Bilthoven, The Netherlands*

[b] *Delft University of Technology, Faculty of Civil Engineering and Geosciences, P.O. Box 5048, 2600 GA Delft, The Netherlands*

[c] *George E. Brown Jr. Salinity Laboratory, USDA, ARS, 450 West Big Springs Road, Riverside, CA, 92 507, USA*

Received 18 December 2000; received in revised form 8 August 2001; accepted 5 September 2001

Abstract

Bacteriophage removal by soil passage in two field studies was re-analyzed with the goal to investigate differences between one- and two-dimensional modeling approaches, differences between one- and two-site kinetic sorption models, and the role of heterogeneities in the soil properties. The first study involved removal of bacteriophages MS2 and PRD1 by dune recharge, while the second study represented removal of MS2 by deep well injection. In both studies, removal was higher during the first meters of soil passage than thereafter. The software packages HYDRUS-1D and HYDRUS-2D, which simulate water flow and solute transport in one- and two-dimensional variably saturated porous media, respectively, were used. The two codes were modified by incorporating reversible adsorption to two types of kinetic sites.

Tracer concentrations were used first to calibrate flow and transport parameters of both models before analyzing transport of bacteriophages. The one-dimensional one-site model did not fully describe the tails of the measured breakthrough curves of MS2 and PRD1 from the dune recharge study. While the one-dimensional one-site model predicted a sudden decrease in virus concentrations immediately after the peaks, measured data displayed much smoother decline and tailing. The one-dimensional two-site model simulated the overall behavior of the breakthrough curves very well. The two-dimensional one-site model predicted a more gradual decrease in virus concentrations after the peaks than the one-dimensional one-site model, but not as good as the one-dimensional two-site model. The dimensionality of the problem hence can partly explain the smooth decrease in concentration after peak breakthrough. The two-dimensional two-site model provided the best results. Values for k_{att2} and k_{det2} could not be determined at the last two of four monitoring wells, thus suggesting that either a second type of kinetic sites is present in the first few meters of dune passage and not beyond the second monitoring well, or that effects of soil heterogeneity and

* Corresponding author. Tel.: +31-30-274-2994; fax: +31-30-274-4434.

E-mail addresses: Jack.Schijven@rivm.nl (J.F. Schijven), Jsimunek@ussl.ars.usda.gov (J. Šimůnek).

[1] Tel.: +1-909-369-4865; fax: +1-909-342-4964.

PII: S0169-7722(01)00188-7

dimensionality of the problem overshadowed this process. Variations between single collector efficiencies were relatively small, whereas collision efficiencies varied greatly. This implies that the nonlinear removal of MS2 and PRD1 is mainly caused by variations in interactions between grain and virus surfaces rather than by physical heterogeneity of the porous medium.

Similarly, a two-site model performed better than the one-site model in describing MS2 concentrations for the deep well injection study. However, the concentration data were too sparse in this study to have much confidence in the fitted parameters.

Keywords: Virus removal; Virus transport; MS2; PRD1; Water treatment; Artificial recharge

1. Introduction

Much interest exists, worldwide, in removing viruses by soil passage, either for protection of groundwater, or as treatment of surface water that is subsequently used for drinking water. Both groundwater as well as surface water may be contaminated with pathogenic viruses from various fecal sources (e.g., Yates, 1985; Havelaar et al., 1993). A considerable amount of research has been carried out on the processes that determine virus removal by soil passage, both at the laboratory and field scale (see Schijven and Hassanizadeh, 2000, for a review). Virus removal during subsurface transport is due to a complex interplay of processes, of which inactivation and adsorption are of major importance (Yates et al., 1987). In sandy aquifers, adsorption is reversible and kinetically limited, while likely several types of kinetic sites exist (Hassanizadeh and Schijven, 2000). In addition, processes of advection, dispersion and dilution cause spreading of viruses and thus affect virus concentrations.

Transport and removal of viruses even in field studies is often still modeled as a one-dimensional problem, assuming constant and steady-state water flow and considering only longitudinal dispersion (e.g. Bales et al., 1997; DeBorde et al., 1999; Pieper et al., 1997; Ryan et al., 1999; Schijven et al., 1999, 2000). In reality, field situations are generally much more complex because of temporal and spatial variations in water flow velocities, diverging or converging flow lines, the effects of transverse dispersion and dilution. For these reasons a two-dimensional, or even a three-dimensional, transport model may be needed.

Another complication in understanding field-scale virus transport is that removal rates of viruses are often higher initially than further along the transport pathway (Bales et al., 1995; DeBorde et al., 1998; Pieper et al., 1997; Ryan et al., 1999; Schijven et al., 1999, 2000). This may be due to heterogeneity within the soil environment at various scales (Schijven and Hassanizadeh, 2000), such as spatial variations of preferential attachment sites formed by ferric oxyhydroxides (Schijven, 2001; Schijven et al., 2000) or in the soil organic matter content (Schijven, 2001).

In the present study, data on virus removal from two field studies (Schijven et al., 1999, 2000) were re-analyzed with the goal to investigate (1) differences between one- and two-dimensional modeling approaches, (2) differences between one- and two-site kinetic sorption models, and (3) the role of heterogeneities in subsurface hydraulic properties on virus removal. The first study involved removal of bacteriophages MS2 and PRD1 by dune recharge at Castricum, The Netherlands (Schijven et al., 1999), while the second study represented removal of MS2 by deep well injection at Someren, The Netherlands

(Schijven et al., 1999). Details about both studies will be given below. Bacteriophages MS2 and PRD1, used in both field studies, represent the low adsorptive behavior of negatively charged viruses and therefore may represent a relatively worst case scenario in terms of rapid virus transport (Schijven and Hassanizadeh, 2000). This was confirmed by results from column experiments with dune sand from the Castricum field site (Schijven, 2001), which showed that a negatively charged pathogenic virus, Coxsackievirus B4, was removed almost as little as MS2, while a less negatively charged virus, Poliovirus 1, was removed much more effectively.

For our analyses, we used the software packages HYDRUS-1D (Šimůnek et al., 1998) and HYDRUS-2D (Šimůnek et al., 1999), which simulate water flow and solute transport in one- and two-dimensional variably saturated porous media, respectively. The two codes were adapted by incorporating reversible adsorption to two types of kinetic sites. Data from the two field studies were previously analyzed using one-dimensional analytical models, assuming constant flow velocities, a homogeneous soil environment, and constant reaction and transport parameters between the source of bacteriophages and several collecting wells. In this study, we will consider the two-dimensionality of both field problems, two-site kinetic sorption, and the heterogeneity of subsurface.

2. Brief description of field experiments

2.1. Removal of MS2 and PRD1 by dune recharge

Removal of bacteriophages MS2 and PRD1 during dune recharge has been studied at Castricum, The Netherlands. Details of this field experiment and an extensive evaluation of the results are found in Schijven et al. (1999). The site consists of fine aeolian dune sands that form a phreatic aquifer around 10 m thick, with a hydraulic conductivity of about 12 m day^{-1} (at a water temperature of 5 °C) and an effective porosity of approximately 0.35. Surface water infiltrates the sand through a number of parallel canals that are about 120 m apart. Water is produced through rows of wells that are placed along midlines of the canals. Within one of the canals, a 150-m^2 (10×15 m) compartment was constructed using PVC sheeting along wooden poles. The distance from this compartment to extraction well PCQ414 was 63 m, with a water travel time of approximately 40 days as determined by salt tracing. Almost perpendicular to the bank of the canal, six monitoring wells, W1 to W6, were installed up to a distance of 30 m along a flow line to extraction well PCQ414 (Fig. 1). Well screens W1 to W4 were 0.25 m long and well screens W5 and W6 0.50 m long. The well screens were positioned at different depths to locate them along a calculated flow line. Table 1 lists the exact locations of these screens.

Prior to the dosage of the water with bacteriophages, sodium chloride was added to the compartment as a conservative salt tracer to estimate the interstitial flow velocity and the medium dispersivity. The chloride concentration of the water in the compartment was increased in one step from 150 to 750 mg/l and kept at this level for exactly 7 days. This represented an increase of electric conductivity (EC) from 890 to about 2700 μS/cm. For a period of 35 days, the EC was measured at 10 min intervals in the six monitoring wells by means of fixed EC-sensors connected to a data logger.

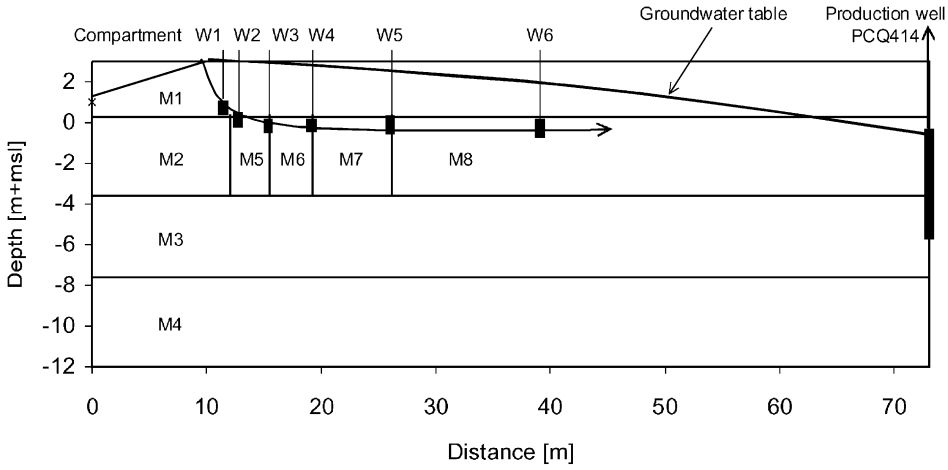

Fig. 1. Schematic cross-section of the dune recharge field site with a source compartment and monitoring wells W1 to W6. The curved arrow indicates the flow path. Depth is given in meters above sea level (msl). M1 to M8 denote the different materials.

Bacteriophages were seeded only after salt concentrations were back to their background levels in order to avoid any possible density effects due to dosage of the salt tracer on estimates of attachment/detachment of bacteriophages. Dosage of the water with phages started by emptying bottles with a phage concentration of 2.5×10^{13} plaque-forming units (pfu) of MS2 and 2.5×10^{12} pfu of PRD1 at the center of the compartment. This was done in order to raise the concentration in the compartment immediately to about 10^8 and 10^7 pfu/l, respectively. Although we tried to keep the concentrations constant by pumping phages from 1000-l containers into the compartment for a period of exactly 11 days, they varied by a factor of about two due to variations in power supply to the dosage pump. Water samples from the compartment and monitoring wells were taken regularly for a period of 4 months. The field study was performed during winter, when water temperatures were low and inactivation hence was minimal. The inactivation rate of phages in the water phase was measured both in the field and by means of laboratory experiments.

Table 1
Location of monitoring screens at the field site for the dune recharge experiment (Vogelaar et al., 1997)

Monitoring screen	Horizontal distance to bank of canal [m]	Top of screen [m+msl]	Bottom of screen [m+msl]	Mean hydraulic head [m+msl]
W1	1.40	0.89	0.64	2.37
W2	2.65	0.3	0.05	2.26
W3	5.30	−0.03	−0.28	2.07
W4	9.05	0.03	−0.22	1.83
W5	15.95	0.17	−0.33	1.44
W6	29.00	0.01	−0.49	0.77

msl is the mean sea level.

Concentrations of MS2 and PRD1 were reduced about 3 $\log_{10}$ within the first 2.4 m and another 5 $\log_{10}$ in a linear fashion within the following 27 m. The higher initial removal rate was investigated in more detail in column experiments (Schijven, 2001). In that study, soil samples were taken at the field site along the same flow line where the monitoring screens were located. These samples were analyzed physicochemically. Grain size distribution showed little variation amongst the soil samples. But the fraction of organic carbon and ferric oxalate, as a measure of ferric oxyhydroxides, decreased exponentially with distance. Following continuous seeding of bacteriophages in 1.4 m columns filled with these different soil materials, concentrations of free bacteriophages were measured every 10 cm along the columns to determine their removal rate with travel time or distance. Bacteriophage removal rates were found to be highly and positively correlated with soil organic carbon content and to a lesser extent with the presence of ferric oxyhydroxides (Schijven, 2001). Hence, we believe that the high initial removal within the first meters of dune passage is due to attachment to preferable sites formed by ferric oxyhydroxides and/or organic carbon.

2.2. Removal of MS2 by deep well injection

Removal of MS2 by deep well injection was studied at a field site near Someren, The Netherlands. Details of this study are given in Schijven et al. (2000). Pre-treated surface water was injected at a depth of 280–310 m below the surface (Fig. 2). A 50-m thick layer of clay overlies the highly permeable aquifer. The aquifer itself lies on top of another 2–3 m thick clay layer. The aquifer consists of several sandy layers (fluvial sediments) that differ in permeability. Water was abstracted at a distance of 98 m from the injection point, from a depth interval of 278–298 m below the surface. Monitoring wells were located at distances of 8 m (WP3), 12 m (WP2), 22 m (WP4) and 38 m (WP1) from the injection well along the line of flow symmetry connecting IP2 and PP1. Samples were taken from 2-m long polyvinyl chloride (PVC) screens at a depth of 310 m below the surface. The screens were all situated within the same layer of sand that had the highest permeability (25 m day^{-1}).

Sodium chloride was injected as a conservative tracer to estimate the interstitial flow velocity of the injected water and the dispersivity of the porous medium. For a period of exactly 5 days, 265 kg NaCl in 880 l was injected each day into the main injection pipeline through which pretreated surface water was injected at a rate of 960 m^3 day^{-1}. This resulted in a salt concentration of 0.275 kg m^{-3} in the injection water, with the electrical conductivity (EC) of the injection water increasing in one step from 450 to about 1000 μS/cm. During the first 2 weeks of the tracer study, the EC was measured automatically at the number-2 screens of IP2, WP3 (8 m) and WP2 (12 m) at 4-h intervals. EC-measurements in samples from the number-2 screens of WP1 (38 m) and WP4 (22 m) were carried out manually at daily and weekly intervals. Similarly as for the dune sand experiment, bacteriophages were seeded only after sodium chloride concentrations were back to their background levels. A phage concentration of 7.0×10^7 pfu/l of MS2 was applied to the injection well for a period of 5 days. The inactivation rate of MS2 in the water phase was measured in a sample from the injection water, and from the water collected after 8 m of soil passage.

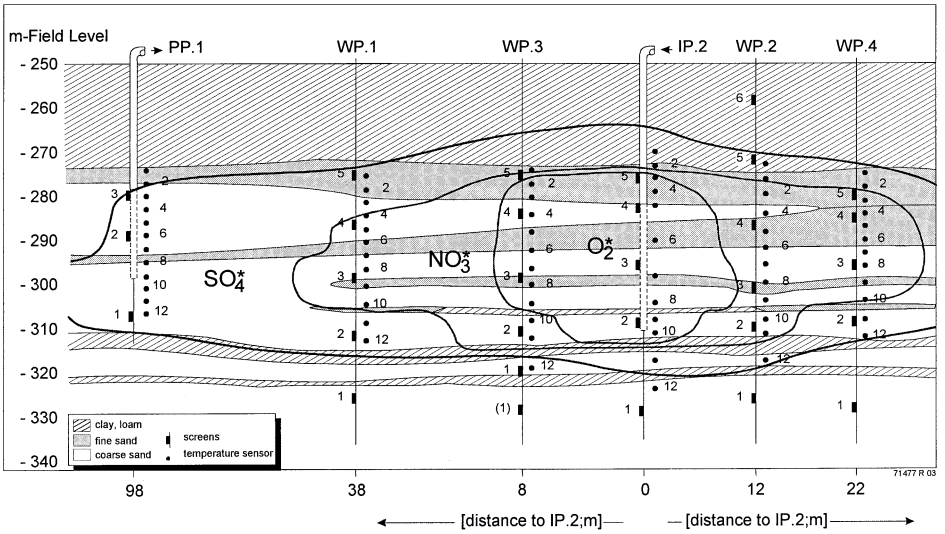

Fig. 2. Schematic cross-section of a field site with injection well IP2, monitoring wells WP1 to WP4 and production well PP1. Samples were taken from the number-2 screens. Also shown are the redox-zones in the aquifer (Stuyfzand, 1999). * O_2 = dissolved oxygen concentration declining with distance from 10 to 0 mg l^{-1}. NO_3 = nitrate concentration declining with distance from 20 to 0 mg l^{-1}. SO_4 = sulfate concentration higher than pretreated surface water due to pyrite oxidation (Schijven et al., 2000).

Within the first 8 m of soil passage, concentrations of MS2 were reduced by 6 $\log_{10}$, but only by about 2 $\log_{10}$ in the following 30 m. From geochemical mass balances, it could be deduced that within the first 8 m distance from the injection well ferric oxyhydroxides precipitated as a consequence of pyrite oxidation, but not at larger distances. Ferric oxyhydroxides provide positively charged patches on to which fast attachment of negatively charged bacteriophages may take place. The non-linear removal could therefore be ascribed to preferable attachment of MS2 to patches of ferric oxyhydroxides that are present within the first 8 m from the injection point, but not thereafter (Schijven et al., 2000).

3. Theory

3.1. Conceptual model

3.1.1. Water flow

Because of the unsaturated nature of part of the transport domain of the dune recharge experiment at Castricum, subsurface flow was simulated with the variably-saturated (Richards') equation as follows

$$\frac{\partial\theta}{\partial t} = \frac{\partial}{\partial x_i}\left[K(h)\left(K_{ij}^{A}\frac{\partial h}{\partial x_j} + K_{iz}^{A}\right)\right] \tag{1}$$

where x_i represents the spatial coordinate [m], with $x_2 = z$ taken here to be positive upward for the vertical cross section (i.e., for dune recharge experiment) and $x_2 = y$ for flow in a horizontal plane (i.e., the deep well injection experiment), t is time [day], θ is the water content [$m^3\ m^{-3}$], h is the pressure head [m], K is the hydraulic conductivity [m day^{-1}], and K_{ij}^{A} are components of a dimensionless anisotropy tensor. Knowledge of the functional relationships relating the water contents and the hydraulic conductivities to the pressure heads, in addition to the initial and boundary conditions, is needed to numerically solve Eq. (1). An advantage of the Richards' equation is that it can be used to describe simultaneously flow in both the saturated and unsaturated zones. Eq. (1) hence can be applied to variably saturated water flow in the dune recharge experiment, and to fully saturated flow in the deep well injection experiment.

3.1.2. Solute and virus transport

Transport of the conservative (NaCl) tracer is described using the convection–dispersion equation. In two-dimensional form, this equation is as follows

$$\frac{\partial \theta c}{\partial t} = \frac{\partial}{\partial x_i}\theta D_{ij}\frac{\partial c}{\partial x_j} - q_i\frac{\partial c}{\partial x_i} \tag{2}$$

where c is the tracer solution concentration [g m^{-3}], q_i is the ith component of the volumetric flux density [m day^{-1}], and D_{ij} is the dispersion coefficient tensor [$m^2\ day^{-1}$] defined as (Bear, 1972)

$$\theta D_{ij} = \lambda_L |q| \delta_{ij} + (\lambda_L - \lambda_T)\frac{q_i q_j}{|q|} + \theta D_d \tau \delta_{ij} \tag{3}$$

where D_d is the molecular diffusion coefficient in free water [$m^2\ day^{-1}$], τ is a tortuosity factor [−], $|q|$ is the absolute value of the Darcian fluid flux density [m day^{-1}], δ_{ij} is the Kronecker delta function, and λ_L and λ_T are the longitudinal and transverse dispersivities [m], respectively.

Schijven et al. (1999) used a one-dimensional (1D) one-site kinetic sorption model to describe the transport of viruses at both field sites. They assumed that both attachment and detachment of viruses to the solid phase could be described using a first-order kinetic rate process. The governing equations describing 1D virus transport are then as follows

$$\theta\frac{\partial C}{\partial t} + \rho_B\frac{\partial S}{\partial t} = \lambda_L\theta v\frac{\partial^2 C}{\partial x^2} - \theta v\frac{\partial C}{\partial x} - \mu_l\theta C - \mu_s\rho_B S \tag{4}$$

$$\rho_B\frac{\partial S}{\partial t} = k_{att}\theta C - k_{det}\rho_B S - \mu_s\rho_B S \tag{5}$$

where C is the concentration of free phages [pfu m^{-3}], S is the concentration of attached phages [pfu kg^{-1}], θ is the water content [$m^3\ m^{-3}$], assumed here to be equal to porosity n [−] for the fully saturated conditions, v ($= q/\theta$) is the average interstitial water velocity [m day^{-1}], ρ_B is the dry bulk density [kg m^{-3}], k_{att} and k_{det} are attachment and

detachment rate coefficients, respectively [day^{-1}]; and μ_l and μ_s are inactivation rate coefficients of the free and attached phages, respectively [day^{-1}]. It was shown that this one-site sorption model could not accurately duplicate the tailing of virus breakthrough curves measured at various monitoring wells (Schijven et al., 1999), nor the breakthrough curves measured on the laboratory samples (Hassanizadeh and Schijven, 2000).

Hassanizadeh and Schijven (2000) showed that the breakthrough curves of bacteriophages MS2 and PRD1 in the column experiments could be better described by means of a convection–dispersion model that incorporates adsorption to two types of kinetic sites. Their model assumes that the sorption sites on the solid phase can be divided into two fractions with different properties and various attachment and detachment rate coefficients. The governing equations of the two-site sorption model are as follows (Hassanizadeh and Schijven, 2000)

$$\theta\frac{\partial C}{\partial t}+\rho_B\frac{\partial S_1}{\partial t}+\rho_B\frac{\partial S_2}{\partial t}=\lambda_L\theta v\frac{\partial^2 C}{\partial x^2}-\theta v\frac{\partial C}{\partial x}-\mu_l\theta C-\mu_{s1}\rho_B S_1-\mu_{s2}\rho_B S_2 \tag{6}$$

$$\rho_B\frac{\partial S_1}{\partial t}=k_{att1}\theta C-k_{det1}\rho_B S_1-\mu_{s1}\rho_B S_1 \tag{7}$$

$$\rho_B\frac{\partial S_2}{\partial t}=k_{att2}\theta C-k_{det2}\rho_B S_2-\mu_{s2}\rho_B S_2 \tag{8}$$

where all variables are the same as for Eqs. (4) and (5), with the subscripts 1 and 2 referring to the two different kinetic sites.

3.2. Numerical model

The governing water flow (Eq. (1)) and solute transport (Eqs. (2)–(8)) equations were solved numerically subject to appropriate initial and boundary conditions using the HYDRUS-1D (Šimůnek et al., 1998) and HYDRUS-2D (Šimůnek et al., 1999) models for the one- and two-dimensional problems, respectively. Galerkin-type linear finite element methods were used for the spatial discretization, and a finite difference method for temporal discretization. A fully implicit mass conservative modified Picard iteration scheme (Celia et al., 1990) was used to solve the Richards' equation.

HYDRUS-1D and HYDRUS-2D simulate water flow and solute transport in variably saturated porous media. The two codes considered the concept of two-site sorption (Selim et al., 1987; van Genuchten and Wagenet, 1989) to permit consideration of nonequilibrium adsorption–desorption reactions. The two-site sorption concept assumes that the sorption sites can be divided into two fractions, with sorption on one fraction of the sites (the type-1 sites) being instantaneous, and with sorption on the remaining (type-2) sites being time-dependent. The HYDRUS codes hence permitted only one type of sorption sites to be kinetic. To make the codes applicable to our study, HYDRUS-1D and HYDRUS-2D were both modified by implementing reversible kinetic adsorption to two sets of kinetic sites as modeled with Eqs. (6)–(8).

3.3. Inverse modeling

Solute transport and reaction parameters, as well as saturated hydraulic conductivities and porosities were obtained by calibrating the HYDRUS-1D and HYDRUS-2D model solutions against the measured data. This was done by iteratively changing model parameters and thus improving model fits to the measured data until a desired degree of precision is obtained. The objective function, SSQ, that was minimized during the parameter estimation procedure contains weighted residuals between the measured data and the model predictions

$$\mathrm{SSQ}(\boldsymbol{b},\boldsymbol{q}) = \sum_{j=1}^{m} \left(v_j \sum_{i=1}^{n_j} w_{ij} \left[q_j^*(\boldsymbol{x},t_i) - q_j(\boldsymbol{x},t_i,\boldsymbol{b}) \right]^2 \right) \tag{9}$$

where the right-hand side represents weighted deviations between the measured and calculated space-time variables (e.g., concentrations and/or pressure heads at different times in the flow domain). In this term, m is the number of different sets of measurements, n_j is the number of measurements in a particular measurement set, q_j^* $(\boldsymbol{x},t_i)$ represents specific measurements at time t_i for the jth measurement set at location $\boldsymbol{x}$,q_j $(\boldsymbol{x},t_i\boldsymbol{b})$ are the corresponding model predictions for the vector of optimized parameters $\boldsymbol{b}$ (e.g., K_s, n, λ_L, k_{att} and k_{det}), and v_j and $w_{i,j}$ are weights associated with a particular measurement set or point, respectively. Minimization of SSQ was accomplished using the Levenberg–Marquardt nonlinear minimization algorithm (Marquardt, 1963).

4. Analysis of the dune recharge experiment

4.1. Water flow and tracer transport

Two types of analyses were carried out with data collected during the dune recharge experiment. First, HYDRUS-1D was used to optimize the hydraulic (i.e., the saturated hydraulic conductivity and porosity) and solute transport (i.e., longitudinal dispersivity and attachment and detachment constants) parameters along a one-dimensional flow path, similarly as in previous studies (Schijven et al., 1999, 2000). In the initial analyses we assumed that the different parameters were constant between the source of tracer or phages and particular wells. However, because model parameters calibrated against data measured at one well often could not reproduce concentrations at the other wells, in later analysis we allowed various variables to vary between individual wells. For comparison purposes we list in Table 2 results obtained previously (Schijven et al., 1999) using the one-dimensional one-site sorption model as modeled with the CXTFIT2 code (Toride et al., 1995). The optimized dispersivities and average pore-water velocities were fitted to the EC and virus data assuming stream tubes from the source to a particular well and with the aquifer having homogeneous properties and constant porosity n of 0.35.

Table 2
Estimated values of model parameters determined using the CXTFIT2 analytical model (one-dimensional, one-site kinetic sorption) from individual breakthrough curves of NaCl, MS2 and PRD1 for the dune recharge experiment (Schijven et al., 1999)

Solute	Variable	Units	Wells					
			W1	W2	W3	W4	W5	W6
	X	m	2.4	3.8	6.4	10.2	17.1	30.1
NaCl	v	m day^{-1}	1.41	1.56	1.59	1.57	1.52	1.19
	λ_L^*	m	0.008	0.012	0.017	0.017	0.0096	0.08
MS2	μ_l	day^{-1}	0.03	0.03	0.03	0.03	0.03	0.03
	μ_s	day^{-1}	0.085	0.092	0.092	0.092	0.092	0.092
	k_{att}	day^{-1}	4.1	3.2	2.8	2.0	1.3	0.8
	k_{det}	day^{-1}	0.00087	0.0016	0.0026	0.0018	0.00052	0.0030
PRD1	μ_l	day^{-1}	0.12	0.12	0.12	0.12	0.12	0.12
	μ_s	day^{-1}	0.071	0.067	0.067	0.067	0.067	0.067
	k_{att}	day^{-1}	4.0	3.1	2.2	1.5	1.3	0.7
	k_{det}	day^{-1}	0.00077	0.0011	0.0018	0.0025	0.0021	0.0034

X is the distance along a streamline.

Table 3 presents stream-tube dispersivities and average pore-water velocities as fitted with the HYDRUS-1D code to the measured EC data. As expected, the optimization results are almost identical to those in Table 2, thus verifying the numerical solution in the HYDRUS-1D code. Optimized pore-water velocities were smaller for the first well (W1), almost constant for the next four wells, and then significantly lower for the last well (W6). The optimized longitudinal dispersivities were very small (on the order or 1 cm) with the exception of the last well, for which we obtained a dispersivity of 8 cm. Although excellent agreement was obtained between measured and fitted concentrations for a particular well (not shown), the optimized parameters could not always be used successfully to predict concentrations at other locations.

To improve the description of concentrations at all wells simultaneously, in the second step of our one-dimensional analyses we assumed that several variables could change between different wells. We used this simplified conceptual model of heterogeneity, i.e., based on the location of wells, because our physical and geochemical analyses of soil

Table 3
One-dimensional optimizations using EC data from the dune recharge experiment and assuming stream tubes from a source to a particular well having constant properties ($n = 0.35$). Each breakthrough curve was optimized independently using HYDRUS-1D

Well	q [m day^{-1}]	λ_L [m]	v [m day^{-1}]	SSQ
W1	0.49 ± 0.001	0.0069 ± 0.0005	1.4	0.0020
W2	0.54 ± 0.001	0.010 ± 0.0007	1.54	0.0043
W3	0.55 ± 0.0015	0.016 ± 0.0016	1.57	0.013
W4	0.56 ± 0.0008	0.016 ± 0.001	1.6	0.0069
W5	0.53 ± 0.0008	0.0074 ± 0.0004	1.51	0.030
W6	0.41 ± 0.0008	0.083 ± 0.0054	1.17	0.033

samples from different locations did not show significant differences between samples and it appeared that the sand was physically relatively homogeneous. Thus, we did not have evidence for a more complex physically based model of soil heterogeneity. We defined an objective function using EC breakthrough curves from all six wells, assumed a constant water flux in the subsurface equal to the arithmetic average of the fluxes in Table 3, used longitudinal dispersivities between individual wells equal to those optimized for particular breakthrough curves, and optimized the porosities between the source and the first well, and between all subsequent two consecutive wells. Although the pore-water velocities could vary along a stream tube depending upon the porosity, the volumetric flux q must be constant unless sources or sinks are present. This optimization assumes that instead of using different stream tubes with particular pore velocities and dispersivities for each well, the solute arriving at the first well is moved further to the second well (with different porosities and dispersivities between the first two wells), and then to the third well, etc. Parameters derived in this way represent effective parameters, characteristic of transport domains between particular wells. Results of the optimization are given in Table 4 and in Fig. 3. Notice an excellent correspondence between the measured and fitted EC data using this simplified model for describing heterogeneity of the experimental site. We obtained a large value of porosity between wells W5 and W6 (equal to 0.6), which causes a relatively small value of the optimized flux for the breakthrough curve of well W6, including its late arrival time.

For the two-dimensional analyses, the transport domain was first divided into four major material layers: the surface layer M1 (from 3.0 to 0.4 m relative to the mean see level), two intermediate layers M2 (0.4 to -3.5 m) and M3 (-3.5 to -7.5 m), and the less permeable layer M4 (-7.5 to -12 m) at the bottom of the transport profile (Fig. 1). These four layers were determined from bore profiles (Vogelaar et al., 1997). As boundary conditions, we used a constant head in the source pool, corresponding to the height of the ponded water, and a constant flux along the active part of the pumping well, corresponding to the pumping rate. Next we calibrated HYDRUS-2D by optimizing the saturated hydraulic conductivities for these boundary conditions against the mean hydraulic heads recorded for all six wells. Defining the objective function using only the mean hydraulic heads in the observation wells produced conductivities that predicted unrealistic arrival times for the tracer fronts at these monitoring wells. Thus, in the next step, we defined the objective function using also values of the mean flux along the streamline as obtained from the one-dimensional analysis of the tracer fronts. This

Table 4
One-dimensional optimization using EC data from the dune recharge experiment and assuming the presence of one stream tube from the source through all wells

Well	W1	W2	W3	W4	W5	W6	SSQ
Porosity	0.384 ± 0.0020	0.282 ± 0.0044	0.338 ± 0.0026	0.352 ± 0.0022	0.371 ± 0.0011	0.596 ± 0.0013	0.00115

All EC data were analyzed simultaneously using HYDRUS-1D; porosities and dispersivities varied between wells. For dispersivities, see Table 3.

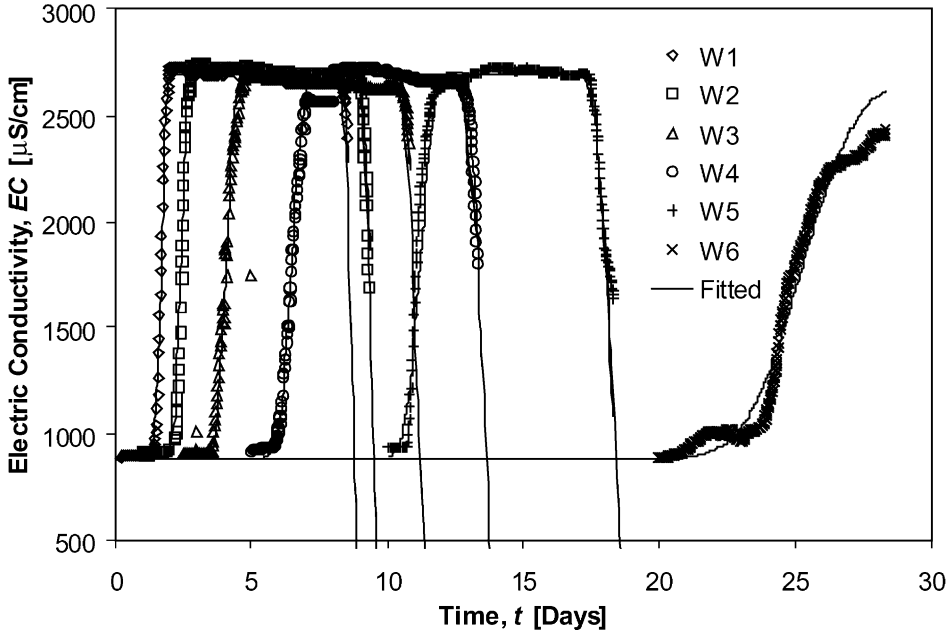

Fig. 3. Measured and optimized EC data assuming a stream tube from the source through all wells of the dune recharge experiment. All EC data were analyzed simultaneously using HYDRUS-1D; porosities and dispersivities varied between wells.

calibration led to the saturated hydraulic conductivities for particular soil layers as given in Table 5 for materials M1 through M4.

In order to obtain better description of the EC breakthrough curves at particular monitoring wells, material layer M2 was further subdivided into another five submaterials (M2, M5, M6, M7 and M8), corresponding to areas between individual wells. We did this additional subdivision only for material layer M2 since this was the only layer for which we had information on NaCl and phages concentrations. Material M2 was situated between the left side of the transport domain and well W2, material M5 was between wells W2 and W3, M6 between W3 and W4, M7 between W4 and W5, and material M8 to the right of well W5 (Fig. 1). We then calibrated the porosities of each of these materials

Table 5
Two-dimensional simulations of EC data from the dune recharge experiment. All EC data were analyzed simultaneously using HYDRUS-2D

Material	M1	M2	M5	M6	M7	M8	M3	M4
K_s [m day^{-1}]	9.55 ± 1.84	11.2 ± 1.71	11.2 ± 1.71	11.2 ± 1.71	11.2 ± 1.71	11.2 ± 1.71	26.0 ± 4.40	2.0
Porosity	0.388 ± 0.0078	0.308 ± 0.060	0.419 ± 0.021	0.403 ± 0.0187	0.326 ± 0.0100	0.502 ± 0.0081	0.350	0.350

using all measured breakthrough curves simultaneously. The results of the two-dimensional analyses of water flow and the EC data are given in Table 5. The optimizations produced similar agreement between measured and optimized NaCl breakthrough curves as those given in Fig. 3 for the one-dimensional numerical analysis.

Calibrated values of the saturated hydraulic conductivity, porosity and longitudinal dispersivity were assumed to correctly describe the solute transport system and were used in our subsequent analyses of virus transport.

4.2. Analysis of virus transport

In the case of the dune recharge study, the measured inactivation coefficients of free bacteriophages, as well as the inactivation coefficients of attached bacteriophages, determined from the slope of the tails of the breakthrough curves, were reported by Schijven et al. (1999). The inactivation rate coefficients of virus attached to site 2 were

Table 6
Parameter values for MS2 breakthrough curves for the dune recharge experiment

	k_{att1}	k_{det1}	k_{att2}	k_{det2}	SSQ	η[a]	α[b]
1D One-site							
W1	4.48 ± 0.170	0.00195 ± 0.00050			0.0391	0.53	1.4×10^{-3}
W2	0.548 ± 0.241	$3.6 \times 10^{-8} \pm 0.0061$			0.0386	0.66	8.1×10^{-5}
W3	2.50 ± 0.105	0.0121 ± 0.00270			0.0140	0.58	5.6×10^{-4}
W4	0.822 ± 0.0887	0.0252 ± 0.0120			0.0135	0.60	2.1×10^{-4}
1D Two-site							
W1	4.28 ± 0.0969	0.000862 ± 0.00020	0.838 ± 0.231	0.0413 ± 0.135	0.0188	0.53	1.3×10^{-3}
W2	0.585 ± 0.173	1×10^{-6}[c] ± 0.00006	0.963 ± 1.55	2.10 ± 6.58	0.0269	0.66	8.6×10^{-5}
W3	2.17 ± 0.0708	0.003110 ± 0.00096	0.0001[c] ± 0.406	NA	0.0058	0.58	4.8×10^{-4}
W4	0.827 ± 0.0666	0.0150 ± 0.0069	0.0001[c] ± 1.56	NA	0.0112	0.60	2.1×10^{-4}
2D One-site							
W1	5.87 ± 0.161	0.00132 ± 0.00028				0.52	1.8×10^{-3}
W2	0.415 ± 0.143	0.181 ± 0.0885			0.0295[d]	0.37	1.4×10^{-4}
W3	1.74 ± 0.0756	0.00209 ± 0.00186				0.42	6.1×10^{-4}
W4	0.0001 ± 1.59	NA			0.0324[d]	0.49	3.3×10^{-8}
2D Two-site							
W1	4.51 ± 0.278	0.00132 ± 0.00042	1.45 ± 0.363	0.215 ± 0.0759		0.52	1.4×10^{-3}
W2	0.447 ± 0.321	0.00202 ± 0.00538	0.0001 ± 0.486	NA	0.0175[d]	0.37	1.5×10^{-4}
W3	1.57 ± 3.50	0.00804 ± 0.0209	0.291 ± 6.84	52.1 ± 1086.9		0.42	5.5×10^{-4}
W4	0.0001 ± 1.05	NA	0.0001 ± 0.550	NA	0.0183[d]	0.49	3.3×10^{-8}

One stream tube from source through all wells was considered in one-dimensional optimizations. Optimizations were carried out sequentially from well to well.

[a] Single collector efficiency.

[b] Collision efficiency associated with k_{att1}.

[c] Parameter fixed or constraint reached.

[d] In the 2D case, breakthrough curves from wells W1 and W2 (and W3 and W4) were optimized simultaneously.

assumed to be the same as those for site 1. All inactivation coefficients were assumed to be known and were not further included in the inverse analysis. The observations were assumed to be log-normally distributed and hence logarithmically transformed prior to the fitting procedure.

Application of the one-dimensional one-site kinetic sorption stream-tube transport model produced a reasonable fit of the breakthrough curves except for considerable discrepancy at the end of the rising and the start of the declining limbs of the breakthrough curves (Schijven et al., 1999). Table 2 lists the corresponding parameter values.

The measured MS2 and PRD1 breakthrough data were subsequently analyzed with the one- and two-dimensional HYDRUS-1D and HYDRUS-2D models using both the one-site and two-site kinetic sorption models. Attachment and detachment coefficients were again optimized sequentially starting with the breakthrough curve measured at well W1, then moving forward to well W2, and so on. In several optimization runs model

Table 7
Parameter values for PRD1 breakthrough curves for the dune recharge experiment

	k_{att1}	k_{det1}	k_{att2}	k_{det2}	SSQ	η[a]	α[b]
1D One-site							
W1	4.56 ± 0.153	0.00217 ± 0.000052			0.051	0.30	2.5×10^{-3}
W2	0.280 ± 0.308	$1 \times 10^{-6} \pm 0.0129$			0.062	0.37	7.41×10^{-5}
W3	1.57 ± 0.136	0.0353 ± 0.000892			0.027	0.33	6.2×10^{-4}
W4	120 ± 617	167 ± 898			0.062	0.33	5.4×10^{-2}
1D Two-site							
W1	4.45 ± 0.0927	0.00116 ± 0.00022	0.876 ± 0.243	0.524 ± 0.170	0.026	0.30	2.4×10^{-3}
W2	0.517 ± 0.247	0.00583 ± 0.00638	1.42 ± 1.33	1.86 ± 3.36	0.0435	0.37	1.4×10^{-4}
W3	0.975 ± 0.0741	0.00756 ± 0.00302	0.442 ± 0.460	1.230 ± 1.76	0.00153	0.33	3.9×10^{-4}
W4	36.8 ± 682	56.8 ± 1071	0.101 ± 0.101	0.00942 ± 0.0481	0.0624	0.33	1.7×10^{-2}
2D One-site							
W1	5.59 ± 0.298	0.00175 ± 0.00056			0.0622	0.29	3.1×10^{-3}
W2	0.471 ± 0.222	0.0302 ± 0.0166			0.0622[c]	0.21	2.7×10^{-4}
W3	0.215 ± 0.304	0.536 ± 1.47				0.24	1.3×10^{-4}
W4	0.001[d]	8.1×10^{8}			0.0910[c]	0.27	6.0×10^{-8}
2D Two-site							
W1	4.90 ± 0.393	0.00175 ± 0.00078	0.961 ± 0.475	0.282 ± 0.2403	0.0139	0.29	2.7×10^{-3}
W2	0.437 ± 1.804	0.00840 ± 0.0437	$0.001^{d} \pm 3.55$	NA	0.0517[c]	0.21	2.5×10^{-4}
W3	0.181 ± 0.296	0.162 ± 0.631	$0.001^{d} \pm 0.687$	NA		0.24	1.1×10^{-4}
W4	0.818 ± 410.5	88.2 too large	$0.001^{d} \pm 2.05$	NA	0.103[c]	0.27	4.9×10^{-4}

One stream tube from source through all wells was considered in one-dimensional optimizations. Optimizations were carried out sequentially from well to well.

[a] Single collector efficiency.

[b] Collision efficiency associated with k_{att1}.

[c] In the 2D case, breakthrough curves from wells W1 and W2 (and W3 and W4) were optimized simultaneously.

[d] Parameter fixed or constraint reached.

parameters were determined simultaneously from two corresponding breakthrough curves. Optimized parameter values determined from the MS2 and PRD1 breakthrough curves, using both one- and two-dimensional analyses and one- and two-site kinetic sorption models, are given in Tables 6 and 7, respectively. Measured and optimized MS2 and PRD1 breakthrough curves for the different models and viruses are presented in Figs. 4–7.

The description of all breakthrough curves using models of various dimensionality and complexity is reasonably good. However, as can be seen from Figs. 4 and 6, the one-dimensional one-site model does not completely describe the tails of the measured breakthrough curves. While the one-dimensional one-site model predicts a sudden decrease of virus concentrations immediately after their peak, measured data display a relatively smooth transition of the declining limb to the more straight later part of the tail. The one-dimensional two-site model did fit the overall shape of the breakthrough curves very well (Figs. 4 and 6).

Figs. 5 and 7 show fits obtained using the two-dimensional model and assuming one-site sorption. The two-dimensional one-site model predicted a more gradual decrease of the virus concentrations after the peaks than the one-dimensional one-site model, but not as good as the one-dimensional two-site model. While the two-dimensional one-site

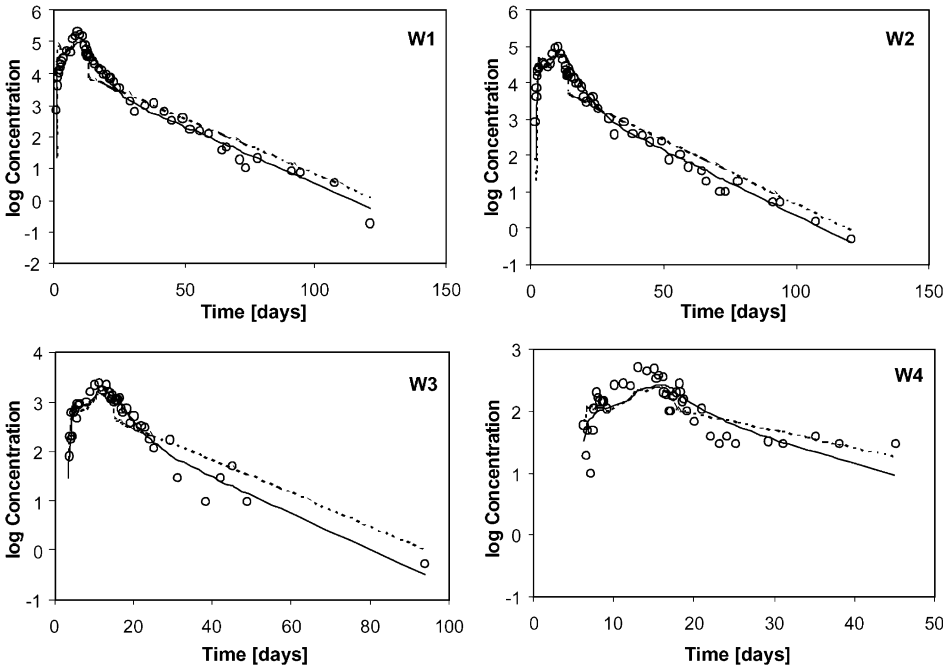

Fig. 4. Measured and optimized MS2 breakthrough curves for the dune recharge experiment. One-dimensional one- and two-site models were used in sequential optimizations. Dots are observations; lines are the model fits (dashed lines for a one-site model, full lines for a two-site model).

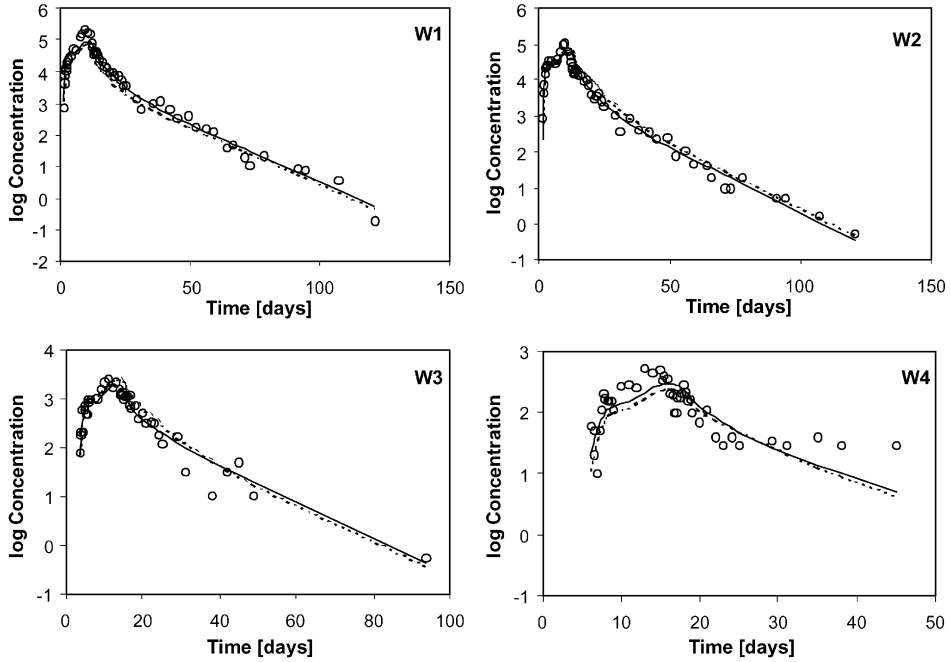

Fig. 5. Measured and optimized MS2 breakthrough curves for the dune recharge experiment. Two-dimensional one- and two-site models were used in sequential optimizations. Dots are observations; lines are the model fits (dashed lines for a one-site model, full lines for a two-site model).

model seems to follow the course of the MS2 tail reasonably well, this is less so for PRD1. Apparently, dimensionality of the problem can partly explain the smoother appearance of the concentration after peak breakthrough. Still, the two-dimensional two-site model fitted (visually as well as based on SSQ values) the breakthrough curve better.

With the two-site model, both one- and two-dimensional, estimates of k_{att2} and k_{det2} for MS2 and PRD1 at W2 were highly uncertain and irregular. The value of k_{att1} at W2 for both MS2 and PRD1 was relatively low, thus suggesting that little adsorption occurred in the vicinity of W2. This may explain the large uncertainty found in the estimates of k_{det2} at W2. Notice also that the models fitted the maximum breakthrough concentration at W2 very well, but generally underestimated the maximum breakthrough at W1. This is because of the skewness of the climbing limb of the breakthrough curve at W1. At W3 and W4, values for k_{att2} and k_{det2} could not be determined with a two-dimensional model. When the attachment coefficients for the second type of sorption sites were small (often estimated with large confidence intervals) or could not be determined altogether, then obviously also the detachment coefficients could not be determined. This suggests that a second type of kinetic sites is either present only in the first few meters of dune passage (due to the presence of organic carbon), but not beyond W2, or that the effects of soil heterogeneity and dimensionality of the problem

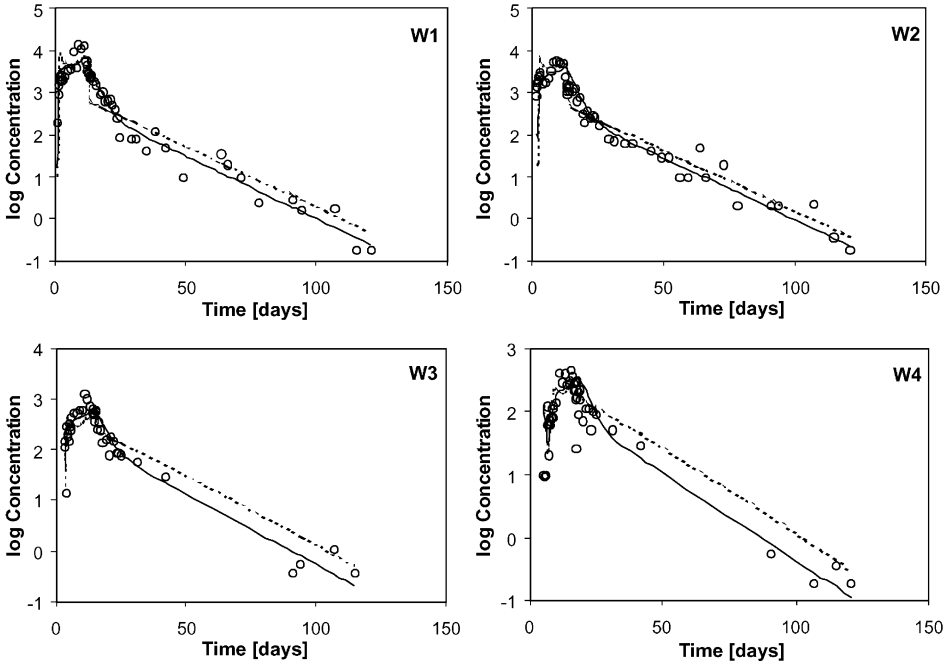

Fig. 6. Measured and optimized PRD1 breakthrough curves for the dune recharge experiment. One-dimensional one- and two-site models were used in sequential optimizations. Dots are observations; lines are the model fits (dashed lines for a one-site model, full lines for a two-site model).

overshadowed this process. The latter explanation seems more plausible since the two-site kinetic sorption process was determined independently on laboratory soil columns (Hassanizadeh and Schijven, 2000). Most of the interaction with the type-1 sites took place before W2, and thus had the greatest effects on the shapes of the breakthrough curves at the subsequent wells. Beyond W2 little attachment took place and the minor changes in the shape of the breakthrough curves are then mainly due to effects of dispersion.

Estimates of k_{att1} between the four different models were quite similar. For both MS2 and PRD1, the highest values were found at W1, reflecting the high initial removal rate that occurred within the first few meters of dune recharge. The other estimates of k_{att1} were lower, varying between 0.0 and 2.5. These variations reflect differences in adsorption properties of the soil and determine variations in removal rates. No attachment could be determined between wells W3 and W4 using a two-dimensional model for both bacteriophages. When modeling breakthrough from the source to a particular well, the variations in rates were less explicit (see Table 2). This is because the higher initial attachment rate was redistributed along the entire stream tube, which leads to gradually decreasing attachment coefficients for wells further along the streamline.

Tables 6 and 7 also list corresponding single collector and collision efficiencies associated with k_{att1}. The single collector efficiency is the rate at which particles, in our

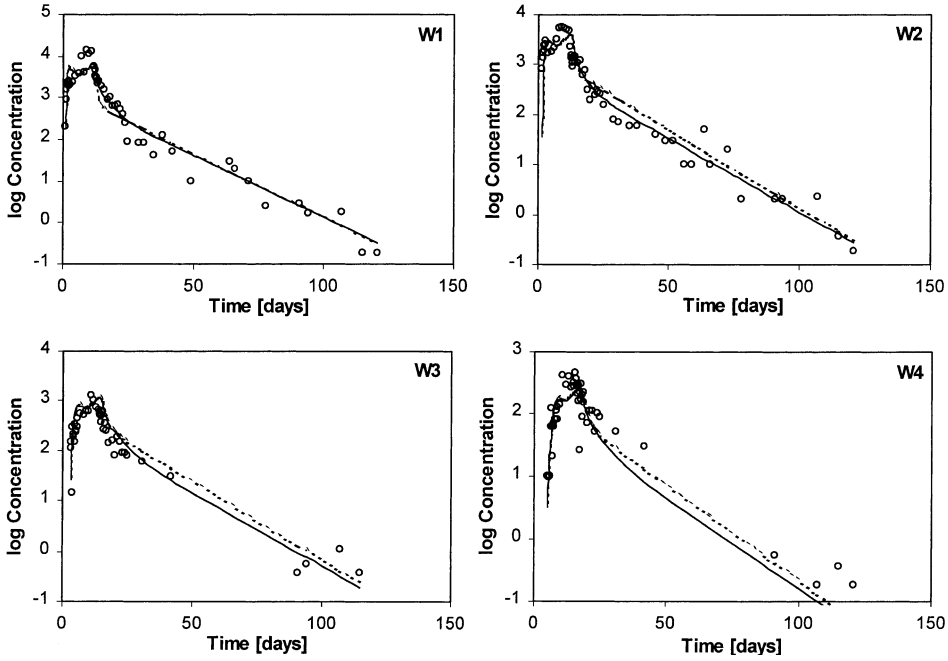

Fig. 7. Measured and optimized PRD1 breakthrough curves for the dune recharge experiment. Two-dimensional one- and two-site models were used in sequential optimizations. Dots are observations; lines are the model fits (dashed lines for a one-site model, full lines for a two-site model).

case viruses, strike a soil grain divided by the rate at which particles move towards the grain and represents the physical factors determining particle collision. The collision efficiency is the efficiency with which collided particles remain attached to the soil grains due to electrostatic interaction. Collision efficiency α was calculated using the following equation (Yao et al., 1971)

$$\alpha = \frac{2}{3}\frac{d_c}{(1-\theta)}\frac{k_{att1}}{v}\frac{1}{\eta} \tag{10}$$

where d_c is the size of the sand grains. The single collector efficiency η was calculated as described by Martin et al. (1992). For each well, velocity at that well was used for calculation of the single collector efficiency.

Variations between single collector efficiencies were relatively small, whereas collision efficiencies varied greatly. This implies that the nonlinear removal of MS2 and PRD1 is mainly caused by variations in the interactions between grain and virus surfaces, rather than by physical heterogeneities of the porous medium. This is in agreement with findings from the column experiments (Schijven, 2001) where removal was found to be strongly and positively correlated with such surface characteristics as soil organic carbon content and ferric oxyhydroxide content.

5. Deep well injection experiment

5.1. Analyses of water flow and tracer transport

Because of the dimensionality of this problem, only two-dimensional modeling was considered. We simulated the deep well injection experiment on a horizontal quadrilateral transport domain of 200 × 100 m that was perpendicular to the monitoring, pumping and injecting wells. The transport domain was discretized into two finite element meshes (3508 and 13 136 finite elements) with a very fine spatial discretization around the injecting and pumping wells and in the area between the two wells. Coarser discretizations were used towards the external boundaries. Wells IP2 and PP1 were simulated as circles with a diameter of 80 cm and were discretized using 15 or 25 nodes for the coarser and finer finite element mesh, respectively. A finer finite element mesh was used for simulation of NaCl transport because the small dispersivities and the absence of sorption and inactivation led to relatively large Peclet numbers over the transport domain, a situation that usually leads to significant numerical oscillations. Coarser meshes could be used for the virus transport calculations since the sorption and inactivation produced considerably smoother (dispersed) curves.

Injection and pumping rates (13 m day $^{-1}$) were used as boundary conditions for water flow, and relative concentrations of injected water for solute transport. NaCl concentrations measured at wells WP2, WP3, and WP4 were used to calibrate the longitudinal dispersivity of the aquifer. The transverse dispersivity was assumed to be one tenth of the longitudinal dispersivity. Results of the calibration for the optimized value of the longitudinal dispersivity of 0.163 cm are shown in Fig. 8. Note that without any calibration of the water flow field, the fit of the first two breakthrough curves was excellent, while only third breakthrough curve arrived slightly later than calculated. Also notice that the tracer not only moved in the direction of the pumping well (monitoring well WP3), but also in the opposite direction (monitoring wells WP2 and WP4). Good calibration of the tracer breakthrough curves at wells WP2 and WP3 should be adequate for our subsequent virus transport analysis. The breakthrough curves for MS2 at WP1 and WP4 were not analyzed because of the limited number of measurements at these wells.

5.2. Analysis of virus transport

Calibrated value of the longitudinal dispersivity and the independently determined saturated hydraulic conductivity and porosity were used as starting points of the virus transport analyses. Again, both one-site and two-site kinetic sorption models were used in the analyses of the MS2 breakthrough curves at wells WP2 and WP3. Optimization results for both models are given in Table 8 and in Fig. 9. In one set of optimization runs, we assumed that the transport parameters are constant throughout the subsurface. In the second set of optimization runs, we allowed the immobilization, attachment, and detachment coefficients to be different in the direction of each well. The second set of optimizations we ran only for the one-site kinetic sorption model.

Similarly as for the dune recharge study, the two-site model performs better than the one-site model in predicting the measured MS2 concentrations, both in terms of the peak

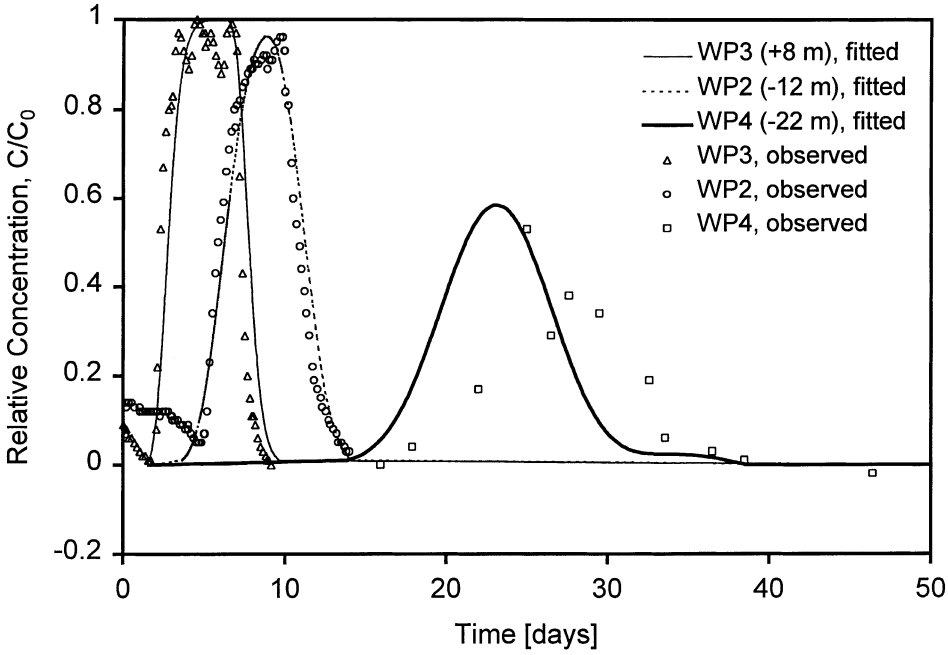

Fig. 8. Measured and optimized NaCl breakthrough curves at three wells for the deep well injection experiment. The distance in the legend corresponds with the location of the monitoring well with respect to the injection and pumping well, with positive number corresponding with monitoring well located between the two major wells.

concentration and subsequent declining concentrations (Fig. 9). Also, similarly as for the dune recharge study, the sum of the attachment coefficients k_{att1} and k_{att2} for the two-site model is approximately equal to the attachment coefficient k_{att1} for the one-site model. Attachment to the type-2 sites is again significantly slower than attachment to the type-1 sites, with detachment from the type-2 sites faster than that from the type-1 sites. This

Table 8
Parameter values for MS2 breakthrough curves for the deep well injection experiment

Model	μ_l	μ_s	k_{att1}	k_{det1}	k_{att2}	k_{det2}	SSQ
One-site (2 wells simultaneously)	0.039[a]	0.163 ± 0.0812	6.276 ± 0.597	0.0165 ± 0.0206			0.672
Two-site (2 wells simultaneously)	0.039[a]	0.0551 ± 0.438	4.91 ± 5.30	0.00170 ± 0.0143	1.68 ± 6.12	0.479 ± 2.01	0.599
One-site (1st well)	0.039[a]	0.112 ± 0.0487	5.85 ± 0.187	0.00278 ± 0.00210			0.0789
One-site (2nd well)	0.039[a]	0.121 ± 0.065	2.49 ± 0.060	0.000366 ± 0.00050			0.0690

[a] Parameter fixed.

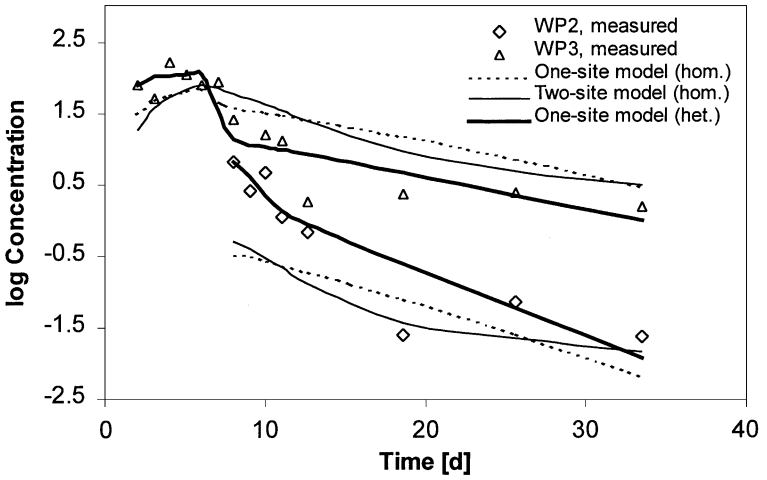

Fig. 9. Measured and optimized MS2 breakthrough curves at two observation wells for the deep well injection experiment assuming homogeneous and heterogeneous subsurface. Two-dimensional one-site and two-site kinetic sorption models were used in the optimization.

leads to a much larger residence time for MS2 on the type-1 sites and more MS2 becoming attached to these sites compared to sites-2. Thus, again, attachment to type-1 sites mainly determines virus removal. Because of the sparseness of MS2 data, the confidence of optimized parameters is relatively small, especially for the two-site model. The estimates of μ_s from the one-site model are very high and likely an overestimation, whereas that from the two-site model approximates that of μ_l. Possibly the value of μ_s is very similar to that of μ_l, because the tails of the breakthrough curves may be even flatter. This is indicated by the three to four observations that make up the later part of the tails.

Excellent agreement between measured and optimized MS2 concentrations was obtained when we allowed the immobilization, attachment, and detachment coefficients for the one-site kinetic sorption model to vary in the direction of each well (Fig. 9). Obviously, this can be explained by the fact that WP3 (8 m) lies within the oxygen zone, whereas WP2 (12 m) lies outside this zone (Fig. 2). Within the oxygen zone, favorable sites of ferric oxyhydroxides are present, but not beyond that zone (Schijven et al., 2000). The MS2 concentration data were, however, too sparse to fit parameters for the two-site kinetic sorption model with varying parameters in the two directions. Possibly, some improvement may be expected when assuming μ_s is equal μ_l.

6. Concluding remarks

We implemented a reversible two-site kinetic sorption model into the HYDRUS-1D and HYDRUS-2D numerical codes and used the resulting models to analyze the transport

of MS2 and PRD phages in two field studies. Differences between the one- and two-dimensional modeling approaches, differences between the one- and two-site kinetic models, and the role of heterogeneities in the soil properties were investigated.

For the dune recharge experiment, the one-dimensional one-site model did not completely describe the tails of the measured breakthrough curves. While the one-dimensional one-site model predicted a sudden decrease in the virus concentrations immediately after their peaks, measured data displayed a relatively smooth transition of the declining limb to the later straight part of the tail. The one-dimensional two-site model fitted the course of the breakthrough curves very well. The two-dimensional one-site model predicted a more gradual decrease in the virus concentrations after their peaks than the one-dimensional one-site model, but not as good as the one-dimensional two-site model. Because the two-dimensional one-site sorption model could describe the measured breakthrough curves already reasonably well, the breakthrough curves did not provide enough information for successful estimation of two-site sorption parameters. Transverse dispersion seemed to partially explain features of the breakthrough curve that were thought to be the effects of a second type of kinetic sites when the one-dimensional model was used. Apparently, dimensionality of the problem can partly predict the smooth decrease in concentration after peak breakthrough. Still, the two-dimensional two-site model did provide better predictions of the breakthrough curves, partly due to the higher order of freedom (more fitted parameters) of the inverse solution. Values for k_{att2} and k_{det2} could not be determined at the larger distances from the source (third and fourth monitoring wells) using the two-dimensional model, thus suggesting that either a second type of kinetic sites is present within the first few meters of dune passage, but not beyond the second monitoring well, or that effects of soil heterogeneity and dimensionality of the problem overshadowed this process. Variations between single collector efficiencies were relatively small, whereas collision efficiencies varied greatly. This implies that the nonlinear removal of MS2 and PRD1 is mainly caused by variations in interactions between grain and virus surfaces rather than by physical heterogeneity of the porous medium.

Similarly, a two-site model performed better than the one-site model in describing MS2 concentration for the deep well injection study. However, the concentration data were too sparse in this study to have much confidence in the fitted parameters.

Acknowledgements

S.M. Hassanizadeh and M.Th. van Genuchten are greatly acknowledged for their expert comments.

References

Bales, R.C., Li, S., Maguire, K.M., Yahya, M.T., Gerba, C.P., Harvey, R.W., 1995. Virus and bacteria transport in a sandy aquifer, Cape Cod, MA. Ground Water 33, 653–661.

Bales, R.C., Li, S., Yeh, T.C.J., Lenczewski, M.E., Gerba, C.P., 1997. Bacteriophage and microsphere transport in saturated porous media: forced-gradient experiment at Borden, Ontario. Water Resour. Res. 33, 639–648.

Bear, J., 1972. Dynamics of Fluid in Porous Media. Elsevier, New York.

Celia, M.A., Bouloutas, E.T., Zarba, R.L., 1990. A general mass-conservative numerical solution for the unsaturated flow equation. Water Resour. Res. 26, 1483–1496.

DeBorde, D.C., Woessner, W.W., Lauerman, B., Ball, P.N., 1998. Virus occurrence in a school septic system and unconfined aquifer. Ground Water 36, 825–834.

DeBorde, D.C., Woessner, W.W., Kiley, Q.T., Ball, P.N., 1999. Rapid transport of viruses in a floodplain aquifer. Water Res. 33, 2229–2238.

Hassanizadeh, S.M., Schijven, J.F., 2000. Use of bacteriophages as tracers for the study of removal of viruses. In: Dassargues, A. (Ed.), Tracers and Modeling in Hydrogeology. Proceedings of TRAM'2000 held in Liege, Belgium, 23–26 May 2000, pp. 167–174.

Havelaar, A.H., van Olphen, M., Drost, Y.C., 1993. F-specific RNA bacteriophages are adequate model organisms for enteric viruses in fresh water. Appl. Environ. Microbiol. 59, 2956–2962.

Marquardt, D.W., 1963. An algorithm for least-squares estimation of nonlinear parameters. J. Soc. Ind. Appl. Math. 11, 431–441.

Martin, R.E., Bouwer, E.J., Hanna, L.M., 1992. Application of clean bed filtration theory to bacterial deposition in porous media. Environ. Sci. Technol. 26, 1053–1058.

Pieper, A.P., Ryan, J.N., Harvey, R.W., Amy, G.L., Illangasekare, T.H., Metge, D.W., 1997. Transport and recovery of bacteriophage PRD1 in a sand and gravel aquifer: effect of sewage-derived organic matter. Environ. Sci. Technol. 31, 1163–1170.

Ryan, J.N., Elimelech, M., Ard, R.A., Harvey, R.W., Johnson, P.R., 1999. Bacteriophage PRD1 and silica colloid transport and recovery in an iron oxide-coated sand aquifer. Environ. Sci. Technol. 33, 63–73.

Schijven, J.F., 2001. Virus Removal from Groundwater by Soil Passage. Modeling, Field and Laboratory Experiments. Ph.D.-thesis, Delft University of Technology, ISBN 90-646-4046-7.

Schijven, J.F., Hassanizadeh, S.M., 2000. Removal of viruses by soil passage: overview of modeling, processes and parameters. Crit. Rev. Environ. Sci.Technol. 30, 49–127.

Schijven, J.F., Hoogenboezem, W., Hassanizadeh, S.M., Peters, J.H., 1999. Modelling removal of bacteriophages MS2 and PRD1 by dune infiltration at Castricum, the Netherlands. Water Resourc. Res. 35, 1101–1111.

Schijven, J.F., Medema, G., Vogelaar, A.J., Hassanizadeh, S.M., 2000. Removal of microorganisms by deep well injection. J. Contam. Hydrol. 44, 301–327.

Selim, H.M., Schulin, R., Flühler, H., 1987. Transport and ion exchange of calcium and magnesium in an aggregated soil. Soil Sci. Soc. Am. J. 51 (4), 876–884.

Šimůnek, J., Šejna, M., van Genuchten, M.Th., 1998. The HYDRUS-1D software package for simulating the one-dimensional movement of water, heat, and multiple solutes in variably-saturated media. Version 2.0, IGWMC-TPS-70. International Ground Water Modeling Center, Colorado School of Mines, Golden, Colorado, 202 pp.

Šimůnek, J., Šejna, M., van Genuchten, M.Th., 1999. The HYDRUS-2D software package for simulating two-dimensional movement of water, heat, and multiple solutes in variably saturated media. Version 2.0, IGWMC-TPS-53. International Ground Water Modeling Center, Colorado School of Mines, Golden, Colorado, 251 pp.

Stuyfzand, P.J., 1999. Deep well injection in Zuid-Oost Nederland (DIZON). Final report on quality changes during soil passage. Kiwa, Nieuwegein, The Netherlands, report KOA 99.054 (In Dutch).

Toride, N., Leij, F.J., van Genuchten, M.Th., 1995. The CXTFIT code for estimating transport parameters from laboratory or field tracer experiments. Version 2.0. US Salinity Laboratory, Agricultural Research Service, US Department of Agriculture, Riverside, CA, Report No. 137.

van Genuchten, M.Th., Wagenet, R.J., 1989. Two-site/two-region models for pesticide transport and degradation: theoretical development and analytical solutions. Soil Sci. Soc. Am. J. 53, 1303–1310.

Vogelaar, A.J., van Baar, M.J.C., Peters, J.H., Bergsma J., Report of NaCl-tracer experiments in December 1996 at Castricum, 1997 Kiwa, Nieuwegein, The Netherlands, report SWI 97.115 (in Dutch).

Yao, K.M., Habibian, M.T., O'Melia, C.R., 1971. Water and wastewater filtration: concepts and applications. Environ. Sci. Technol. 5, 1105–1112.

Yates, M.V., 1985. Septic tank density and groundwater contamination. Ground Water 23, 586–591.

Yates, M.V., Yates, S.R., Wagner, J., Gerba, C.P., 1987. Modelling virus survival and transport in the subsurface. J. Contam. Hydrol. 1, 329–345.